

# Emergent superconducting stripes in two-orbital superconductors

Qiong Qin<sup>1</sup> and Yi-feng Yang<sup>2,3,4,\*</sup>

<sup>1</sup>*New Cornerstone Science Laboratory, Department of Physics,*

*School of Science, Westlake University, Hangzhou 310024, Zhejiang, China*

<sup>2</sup>*Beijing National Laboratory for Condensed Matter Physics and Institute of Physics,*  
*Chinese Academy of Sciences, Beijing 100190, China*

<sup>3</sup>*University of Chinese Academy of Sciences, Beijing 100049, China*

<sup>4</sup>*Songshan Lake Materials Laboratory, Dongguan, Guangdong 523808, China*

(Dated: August 21, 2025)

Motivated by recent experiments in KTaO<sub>3</sub>/EuO interface, we propose an intrinsic mechanism where superconducting stripes emerge naturally without involving disorder, charge inhomogeneity, or competing orders. Our theory is based on a two-orbital model of superconductivity, where one orbital displays a quasi-one-dimensional dispersion and the other orbital is more localized and contributes pairing interactions along the perpendicular direction. Our auxiliary-field Monte Carlo simulations demonstrate that the pairing amplitude exhibits spatial modulation such that the superconductivity naturally disaggregates into two-leg or three-leg superconducting stripes separated by non-superconducting blocks. Our work provides a promising scenario of emergent superconducting stripes in homogeneous two-dimensional systems and reveals unexpectedly rich physics in two-orbital superconductors for future materials design.

*Introduction.*— Superconducting stripes have been extensively studied in correlated superconductors, e.g., the high- $T_c$  cuprates, and recently reported in SrTa<sub>2</sub>S<sub>5</sub> and KTaO<sub>3</sub>/EuO interface [1–3]. While such phenomena have often been attributed to extrinsic factors such as disorder, strain, or competing magnetic/charge orders, the underlying mechanisms remain inconclusive. In doped Mott insulators, for example, kinetic energy frustration may drive hole-rich rivers bordered by spin-ordered domain. In KTaO<sub>3</sub>/EuO interface, however, no evidence of disorder or charge inhomogeneity has been reported in experiment. An intrinsic mechanism is therefore demanded under which superconductivity may naturally disaggregate into stripes.

In this work, we propose a scenario where superconducting stripes emerge without involving disorder, charge inhomogeneity, or competing orders. Our theory was initially motivated by recent studies of high- $T_c$  bilayer nickelate superconductors [4–10]. While their detailed pairing mechanism is still under debate [11–32], the low-lying physics is generally recognized to arise from two orthogonal orbitals: the almost half-filled  $d_{z^2}$  orbital and nearly quarter-filled  $d_{x^2-y^2}$  orbital [33–41], where the  $d_{z^2}$  orbitals contribute inter-layer pairing interaction and the  $d_{x^2-y^2}$  orbitals show good metallic behavior and hybridize with the  $d_{z^2}$  orbitals [16–18]. As a result, Cooper pairs form along the  $z$  axis but hop within the  $xy$  plane to attain the phase coherence, in sharp contrast to most other superconductors. A phenomenological Ginzburg-Landau analysis has shown that the superconductivity in ideal multilayer ( $\geq 4$ ) systems may naturally decompose into bilayer or trilayer superconducting blocks and exhibit order parameter modulation along the  $z$  axis [42]. However, valence difference or layer imbalance might prevent its occurrence in multilayer nickelates.

In KTaO<sub>3</sub>/EuO interface [3], first-principles calculations also reveal two orthogonal orbitals around the Fermi energy: the spin-polarized  $d_{xy}$  orbital and the itinerant  $d_{yz}$  orbital with quasi-one-dimensional dispersion. These led us to propose an effective two-orbital model in two dimension, where the more localized orbital contributes the pairing along one direction and the more itinerant orbital provides the hopping along the other direction. The two orbitals hybridize between nearest-neighbor sites, which may help induce phase coherence for the superconductivity. In real materials, the model may be realized in multi-chain or square-lattice forms.

Our Monte Carlo simulations confirm the emergence of superconducting stripes in such two-orbital superconductors. Notably, even-chain and square-lattice systems predominantly consist of two-leg superconducting stripes separated by non-superconducting blocks, while odd-chain systems may undergo a phase transition from an entirely two-leg-stripe configuration to one with an additional three-leg stripe. In all cases, superconducting stripes emerge and remain robust without involving disorders, charge inhomogeneity, or competing orders, thus providing a potential explanation of the superconducting stripes observed in two dimensional interface. Our work opens a direction of two-orbital superconductivity for future materials design and experimental investigations.

*Model and Method.*— We consider the two-orbital effective  $t$ - $V$ - $J$  Hamiltonian in multi-chain form [16, 17, 30]:

$$\begin{aligned}
 H = & -t \sum_{lis} (c_{lis}^\dagger c_{l,i+1,s} + h.c.) - \mu \sum_{is} c_{lis}^\dagger c_{lis} \\
 & - V \sum_{lis} \left( c_{lis}^\dagger d_{l,i+1,s} + d_{lis}^\dagger c_{l,i+1,s} + h.c. \right) \\
 & - t_\perp \sum_{ais} \left( d_{ais}^\dagger d_{a+1,is} + h.c. \right) + J \sum_{ai} \mathbf{S}_{ai} \cdot \mathbf{S}_{a+1,i},
 \end{aligned} \tag{1}$$

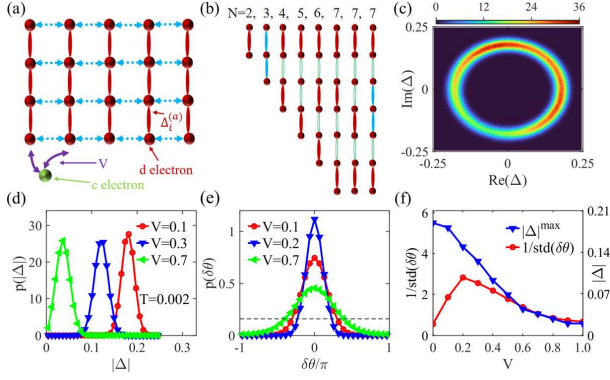


FIG. 1: (a) Schematic representation of the two-orbital model. (b) Illustrations of the stripe configurations for multi-chain systems of  $2 \leq N \leq 7$ . (c) Intensity plot of the probabilistic distribution  $p(\Delta)$  of the local pairing fields on complex plane at  $V = 0.1$  for  $N = 2$ . (d) Probabilistic distribution  $p(|\Delta|)$  of the pairing field amplitude for different  $V$ . (e) Corresponding phase difference distribution  $p(\delta\theta)$  of the pairing fields between two distant bonds for different  $V$ . (f) Evolution of the peak position  $|\Delta|^{\max}$  in  $p(|\Delta|)$  and the inverse standard deviation,  $1/\text{std}(\delta\theta)$ , derived from  $p(\delta\theta)$  with the hybridization  $V$ . All data were obtained at  $T = 0.002$ .

where  $d_{lis}$  ( $c_{lis}$ ) denotes the more localized (itinerant) orbital of spin  $s$  on site  $i$  of chain  $l = 1, 2, \dots, N$ ,  $\mathbf{S}_{li} = \frac{1}{2} \sum_{ss'} d_{lis}^\dagger \boldsymbol{\sigma}_{ss'} d_{lis}$  is the spin operator of the  $d$  electrons, where  $\boldsymbol{\sigma}$  are the Pauli matrices,  $J$  ( $t_\perp$ ) is the superexchange interaction (hopping) of  $d$  electrons between nearest-neighbor chains with  $a = 1, 2, \dots, N-1$ ,  $t$  is the nearest-neighbor hopping of  $c$  electrons along the chain,  $\mu$  is their chemical potential, and  $V$  is the hybridization between two orbitals on nearest-neighbor sites in each chain. All parameters should be considered to have been renormalized by Coulomb repulsions. For simplicity, we assume spin-singlet pairing and ignore all other instabilities. This allows us to utilize the static auxiliary-field Monte Carlo approach, which has been applied to many correlated systems [43–53] and predicted the correct magnitude of  $T_c$  in bilayer and trilayer nickelate superconductors [17, 18].

To perform numerical simulations, we first decouple the superexchange term [54]:

$$J \mathbf{S}_{ai} \cdot \mathbf{S}_{a+1,i} \rightarrow \sqrt{2} \bar{\Delta}_i^{(a)} \Phi_i^a + \sqrt{2} \bar{\Phi}_i^a \Delta_i^{(a)} + \frac{8 \bar{\Delta}_i^{(a)} \Delta_i^{(a)}}{3J}, \quad (2)$$

where  $\Phi_i^a = \frac{1}{\sqrt{2}} (d_{ai\downarrow} d_{a+1,i\uparrow} - d_{ai\uparrow} d_{a+1,i\downarrow})$  represents the inter-chain spin singlet of  $d$  electrons at site  $i$  between  $a$ -th and  $(a+1)$ -th chains and  $\Delta_i^{(a)}$  is the corresponding auxiliary pairing field, as illustrated in Fig. 1(a). To avoid the sign problem, we neglect the imaginary time dependence of the auxiliary fields,  $\Delta_i^{(a)}(\tau) \rightarrow \Delta_i^{(a)} = |\Delta_i^{(a)}| e^{i\theta_i^a}$ , which retains full thermodynamic and spatial fluctuations, thus describing well superconducting

phase fluctuations beyond mean-field approximation [53]. The resulting bilinear form allows us to integrate out all fermionic degrees of freedom and obtain an effective action,  $S_{\text{eff}}(\{\Delta_i^{(a)}\})$ , solely of the pairing fields. Monte Carlo simulations are then performed to sample the probabilistic distribution  $p(\{\Delta_i^{(a)}\}) = Z^{-1} e^{-S_{\text{eff}}(\{\Delta_i^{(a)}\})}$ , where  $Z$  is the partition function serving as the normalization factor. For simplicity, we set  $t = 1$  as the energy unit, fix  $\mu = -1.3$ ,  $J = 0.5$ ,  $T = 0.002$ , and tune  $V$  as the free parameter. For multi-chain systems, we apply periodic boundary condition along the chain direction and open boundary condition perpendicular to the chains. For square lattice, periodic boundary conditions are applied to both directions. The total number of lattice sites ranges from 196 to 210 depending on the lattice geometry. All results have been verified to be qualitatively consistent for larger lattice sizes.

*N = 2.*— As a reference for larger  $N$ , we first study the case  $N = 2$ , a two-leg ladder with pairing interaction on the rung and hopping along both legs. Figure 1(c) plots the distribution  $p(\Delta)$  on the complex plane ( $\text{Re}\Delta, \text{Im}\Delta$ ) for all  $\Delta_i$  at  $V = 0.1$ . The ring shape indicates superconducting phase fluctuations without breaking the global  $U(1)$  symmetry at finite temperature. The amplitude distribution  $p(|\Delta|)$  is given in Fig. 1(d), showing peaks at  $|\Delta|^{\max}$  moving towards smaller values as  $V$  increases. Figure 1(e) plots the distribution of the phase difference  $\delta\theta$  between two distant bonds separated by an extended intra-chain distance of 10 sites. The peak shape centered around  $\delta\theta = 0$  and its width reflect phase correlation and fluctuations along the chain, whose standard deviation,  $\text{std}(\delta\theta) \equiv \sqrt{\langle (\delta\theta)^2 \rangle}$ , is inversely related to the superfluid density. As  $V$  increases, the peak gets narrowed but then broadened, causing nonmonotonic evolution of  $1/\text{std}(\delta\theta)$  plotted in Fig. 1(f), in contrast to the continuous suppression of  $|\Delta|^{\max}$ . This implies a dual role of the hybridization, which tends to induce the phase coherence but at the same time reduce the pairing strength. As a result, the superconductivity at large  $V$  is constrained by the pairing strength, as expected in the weak-coupling BCS theory, but at small  $V$  is governed by phase fluctuations, as studied extensively in underdoped cuprate superconductors [55, 56].

*Even N.*— Figure 2(a) shows  $p(\Delta)$  on complex plane for  $N = 4, 6, 8$  at  $V = 0.1$ . Inside the ring, an additional disk shape appears at the origin, implying thermal fluctuations without pairing. We find two well-separated peaks in  $p(|\Delta|^{(a)})$  for  $N = 4, 6$  in Figs. 2(b) and 2(c), respectively, where  $|\Delta|^{(1,3,5)}$  correspond to the ring and  $|\Delta|^{(2,4)}$  the disk. This indicates spatial modulation of the pairing amplitudes with two-leg superconducting stripes separated by non-superconducting blocks, as illustrated in Fig. 1(b) for  $N = 4, 6$ . This pattern persists for all even-chain systems and extends to the square lattice as shown in Figs. 2(g) and 2(h), where it breaks the

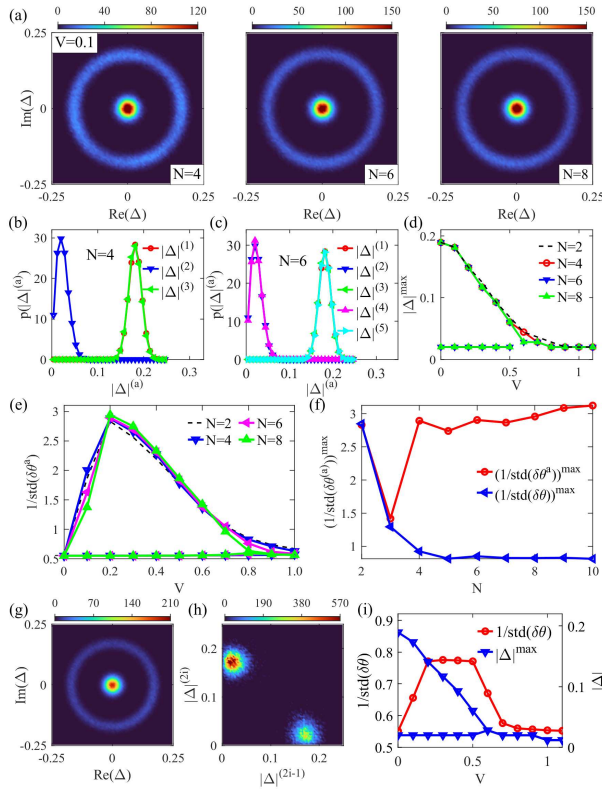


FIG. 2: (a) Intensity plots of the probabilistic distribution  $p(\Delta)$  of the local pairing fields at  $V = 0.1$  for  $N = 4, 6, 8$ . (b) and (c) are the corresponding amplitude distribution  $p(|\Delta|^{(a)})$  for  $N = 4$  and  $6$ , respectively. (d) Peak position  $|\Delta|^{\max}$  of  $p(|\Delta|)$  as a function of the hybridization  $V$  for  $N = 4, 6, 8$ . (e) Evolution of the inverse standard deviation  $1/\text{std}(\delta\theta^a)$  of the phase difference between distant bonds in superconducting and non-superconducting blocks separately. (f) Comparison of the maximum  $1/\text{std}(\delta\theta^a)$  of superconducting blocks and those averaged over all blocks ( $1/\text{std}(\delta\theta)$ ) as functions of  $N$ . (g) Intensity plot of  $p(\Delta)$  at  $V = 0.1$  for the square lattice model. (h) Joint distribution of the pairing amplitudes between two adjacent blocks. (i)  $|\Delta|^{\max}$  and  $1/\text{std}(\delta\theta)$  (calculated over all blocks) as functions of the hybridization  $V$ . The data in (g-i) were produced on a  $14 \times 14$  square lattice.

lattice translational symmetry along the pairing direction. Figure 2(d) shows  $|\Delta|^{\max}$  as a function of  $V$ . As  $V$  increases,  $|\Delta|^{\max}$ , hence the pairing strength, of the superconducting stripes is reduced gradually, and the rest blocks remain non-superconducting. Again, as shown in Fig. 2(e), the inverse phase fluctuation  $1/\text{std}(\delta\theta^a)$  of superconducting blocks varies nonmonotonically with  $V$ . Similar behaviors also exist in the square lattice model as shown in Fig. 2(i). Interestingly, as plotted in Fig. 2(f), the peak values,  $(1/\text{std}(\delta\theta^a))^{\max}$ , of the superconducting blocks vary only slightly with  $N$  except for  $N = 3$ . This suggests that all two-leg superconducting blocks exhibit similar properties insensitive to the whole lattice. By contrast, those of the overall phase distributions de-

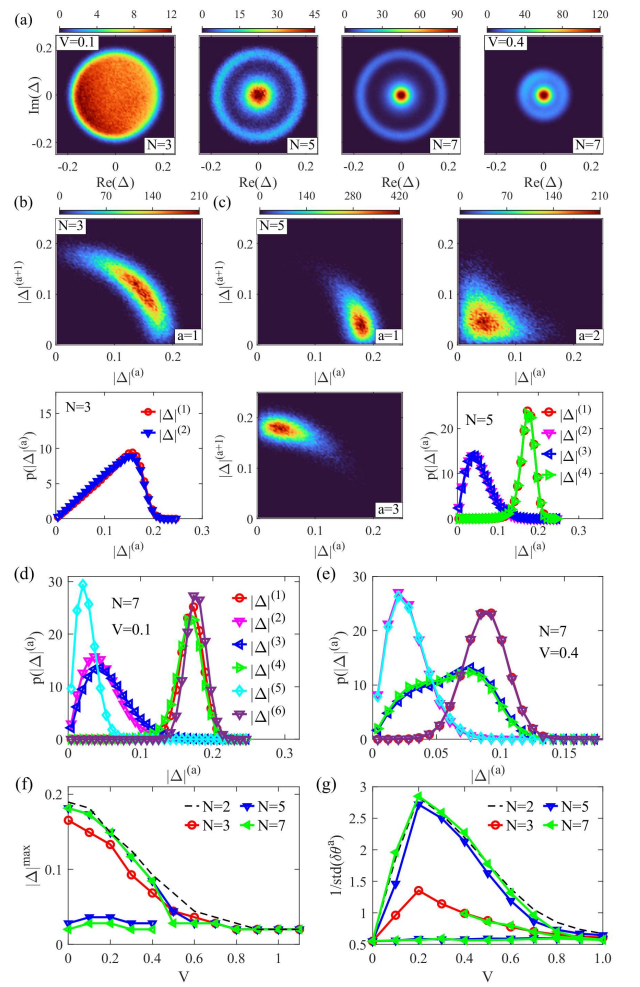


FIG. 3: (a) Intensity plot of  $p(\Delta)$  for  $N = 3, 5, 7$ . (b) and (c) show the amplitude distribution  $p(|\Delta|^{(a)})$  of the local pairing fields and their joint distribution  $p(|\Delta|^{(a)}, |\Delta|^{(a+1)})$  between two nearest-neighbor blocks for  $N = 3$  and  $5$ , respectively. (d) and (e) present  $p(|\Delta|^{(a)})$  for  $N = 7$  at  $V = 0.1$  and  $0.4$ , respectively. (f) and (g) compare the extracted  $|\Delta|^{\max}$  and  $\text{std}(\delta\theta^a)$  with varying hybridization  $V$  for  $N = 2, 3, 5, 7$ .

crease with increasing  $N$  and saturate for  $N \geq 5$  due to the contribution from non-superconducting blocks, indicating stronger inter-block phase fluctuations.

*Odd  $N$ .*— The odd  $N$  cases display very different patterns. Figure 3(a) plots the distribution  $p(\Delta)$  for  $N = 3, 5, 7$ . A broader disk is seen for  $N = 3$ . Correspondingly in Fig. 3(b), the pairing amplitudes of  $a = 1$  and  $2$  blocks exhibit almost identical distributions, with their joint distribution  $p(|\Delta|^{(1)}, |\Delta|^{(2)})$  forming a quarter-ring shape. This implies that both blocks are superconducting but fluctuate strongly around an overall amplitude, since both outer chains tend to form spin singlets with the inner chain. As a result, the phase difference fluctuations are also stronger, explaining the anomalous suppression of  $(1/\text{std}(\delta\theta^a))^{\max}$  for  $N = 3$  in Figs. 2(f) and 3(g).



Similar competition has been proposed for trilayer nickelate superconductors, where the upper and lower layers compete to form spin-singlet pairs with the inner layer, causing a reduced  $T_c$  compared to bilayer nickelates [18].

The distribution  $p(\Delta)$  for  $N = 5$  appears similar to those of  $N = 4$  and 6, except that the central disk is now slightly broadened. Its amplitude distribution is shown in Fig. 3(c). We find that  $|\Delta|^{(1,4)}$  are superconducting and  $|\Delta|^{(2,3)}$  are non-superconducting, giving rise to two superconducting stripes on boundaries separated by a three-leg non-superconducting block in the middle, as illustrated in Fig. 1(b).

For  $N = 7$ , the intensity plot of  $p(\Delta)$  on complex plane reveals two distinct states at small and large  $V$ , with the transition occurring at around  $V = 0.35$  for  $T = 0.002$ . Comparison with the amplitude distribution shown in Fig. 3(d) suggests that the state at small  $V$  is similar to the  $N = 5$  case but with three two-leg superconducting stripes separated by a two-leg non-superconducting block and a three-leg non-superconducting block, while the state at large  $V$  contains two two-leg superconducting stripes on boundaries and one three-leg superconducting stripe (resembling the  $N = 3$  case) in the middle separated by two non-superconducting blocks, as illustrated in Fig. 1(b) for  $N = 7$ . Similar analyses for larger odd  $N$  confirm that two-leg superconducting stripes always emerge at both boundaries. Depending on the location of the three-leg non-superconducting block (small  $V$ ) or three-leg superconducting stripe (large  $V$ ) in the middle, the superconductivity contains  $\frac{N-3}{2}$  or  $\frac{N-5}{2}$  near degenerate configurations, respectively. In all cases, as shown in Figs. 3(f) and 3(g), the extracted  $|\Delta|^{\max}$  exhibits similar suppression with increasing  $V$ , in contrast to the nonmonotonic variation of  $1/\text{std}(\delta\theta^a)$ , again reflecting the crossover between strong- and weak-coupling superconductivity.

**Robustness of stripes.** – For simplicity, we have assumed  $t_\perp = 0$  for the correlated  $d$  orbitals in above calculations. To examine the robustness of the emergent superconducting stripes, we discuss the effect of a finite  $t_\perp$ , whose value is supposed to be strongly renormalized by the on-site Coulomb repulsion and thus small. The results for  $t_\perp = 0.1$  are presented in Fig. 4, showing no significant difference in the distribution for  $N \leq 5$ . For  $N = 6$ , there appears a slight deviation from the peak positions  $|\Delta|^{(a),\max}$  of the inner and outer superconducting blocks, as is seen in Fig. 4(b) above  $t_\perp = 0.08$ . For  $N = 7$ , a finite  $t_\perp$  tends to stabilize the three-leg superconducting stripe in the center and cause the transition between two superconducting states discussed earlier. This is clearly seen in Fig. 4(c), where the peak position of  $|\Delta|^{(3)}$  grows rapidly first and then merges with that of  $|\Delta|^{(4)}$  as  $t_\perp$  increases. Correspondingly in Fig. 4(d), the joint distribution  $p(|\Delta|^{(3)}, |\Delta|^{(4)})$  for  $N = 7$  changes to a quarter-ring shape. This three-leg stripe turns non-superconducting at  $t_\perp \approx 0.12$ , while the two-leg superconducting stripes

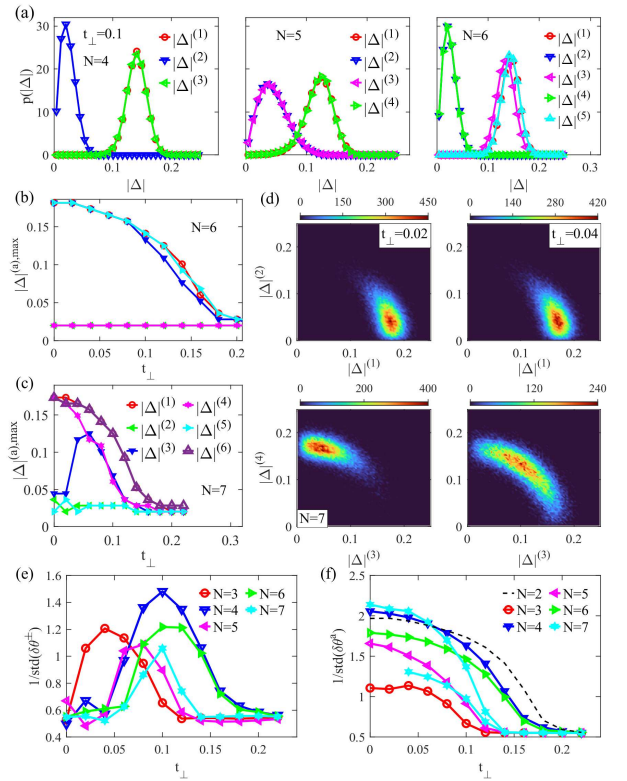


FIG. 4: (a) Amplitude distribution  $p(|\Delta|)$  of the local pairing fields for  $N = 4, 5, 6$  at  $t_\perp = 0.1$ . (b) and (c) show the corresponding peak position,  $|\Delta|^{(a),\max}$ , of the block-dependent amplitude distribution varying with  $t_\perp$  for  $N = 6$  and 7, respectively. (d) Joint distribution  $p(|\Delta|^{(a)}, |\Delta|^{(a+1)})$  between two adjacent blocks at  $t_\perp = 0.02, 0.04$  for  $N = 7$ . (e) and (f) compare the inter-block  $1/\text{std}(\delta\theta^\pm)$  and intra-block  $1/\text{std}(\delta\theta^a)$  of the superconducting stripes as functions of  $t_\perp$  for different  $N$ . All results were obtained at  $V = 0.1$  and  $T = 0.002$ .

on two boundaries persist to a larger  $t_\perp \approx 0.18$ , beyond which the superconductivity is completely destroyed. In all cases, non-superconducting blocks remain almost untouched, confirming the robustness of stripe formation.

The effect of  $t_\perp$  may be further understood from Fig. 4(e), where  $\delta\theta^\pm$  denotes the phase difference between two superconducting blocks. With increasing  $t_\perp$ , the inverse standard deviation  $1/\text{std}(\delta\theta^\pm)$  first increases, marking the gradual development of phase coherence between different superconducting blocks, and then decreases following the continuous suppression of  $1/\text{std}(\delta\theta^a)$  within each superconducting block shown in Fig. 4(e). Thus, while the inter-chain hopping promotes the inter-block phase coherence, it simultaneously reduces the coherence within each superconducting block. For large  $t_\perp$ , the latter constrains the superconducting phase coherence along the perpendicular direction, causing the nonmonotonic evolution of  $1/\text{std}(\delta\theta^\pm)$  shown in Fig. 4(d). Only for sufficiently large  $t_\perp$ , the inter-block  $1/\text{std}(\delta\theta^\pm)$  gets com-

parable to the intra-block  $1/\text{std}(\delta\theta^a)$ , indicating similar phase coherence along both directions. At smaller  $t_\perp$ , the superconductivity remains anisotropic, as observed in experiments [1–3, 57, 58].

*Discussion and conclusions.*—We have proposed an intrinsic mechanism for emergent superconducting stripes without involving disorder, charge inhomogeneity, or competing orders. Our theory is based on a special two-orbital model with the pairing and hopping occurring along perpendicular directions. For even-chain systems or the square lattice, we show that the superconductivity naturally disaggregates into two-leg superconducting stripes separated by non-superconducting blocks, while for odd-chain systems, a phase transition occurs between different stripe patterns. In all cases, the stripe phenomena remain robust. Note that our conclusion does not depend on the special pairing type. It may therefore be readily extended to help understand the emergent superconducting stripes observed in homogeneous two-dimensional systems such as the  $\text{KTaO}_3/\text{EuO}$  interface [3]. The unexpectedly rich physics revealed here will also stimulate future materials design and experimental investigations of two-orbital superconductors.

This work was supported by the National Natural Science Foundation of China (Grants No. 12474136 and No. 12447125).

---

\* yifeng@iphy.ac.cn

- [1] J. M. Tranquada et al., Evidence for unusual superconducting correlations coexisting with stripe order in  $\text{La}_{1.875}\text{Ba}_{0.125}\text{CuO}_4$ , *Phys. Rev. B* **78**, 174529 (2008).
- [2] A. Devarakonda et al., Evidence of striped electronic phases in a structurally modulated superlattice, *Nature* **631**, 526 (2024).
- [3] X. Hua et al., Superconducting stripes induced by ferromagnetic proximity in an oxide heterostructure, *Nat. Phys.* **20**, 957 (2024).
- [4] H. Sun, M. Huo, X. Hu, J. Li, Z. Liu, Y. Han, L. Tang, Z. Mao, P. Yang, B. Wang, J. Cheng, D.-X. Yao, G.-M. Zhang, and M. Wang, Signatures of superconductivity near 80 K in a nickelate under high pressure, *Nature* **621**, 493 (2023).
- [5] J. Hou et al., Emergence of high-temperature superconducting phase in pressurized  $\text{La}_3\text{Ni}_2\text{O}_7$ , *Chinese Phys. Lett.* **40**, (2023).
- [6] Y. Zhang et al., High-Temperature superconductivity with zero resistance and strange-metal behaviour in  $\text{La}_3\text{Ni}_2\text{O}_{7-\delta}$ , *Nat. Phys.* **20**, 1269 (2024).
- [7] N. Wang et al., Bulk high-temperature superconductivity in pressurized tetragonal  $\text{La}_2\text{PrNi}_2\text{O}_7$ , *Nature* **634**, 579 (2024).
- [8] Q. Li, Y. J. Zhang, Z. N. Xiang, Y. Zhang, X. Zhu, and H. H. Wen, Signature of superconductivity in pressurized  $\text{La}_4\text{Ni}_3\text{O}_{10}$ , *Chinese Phys. Lett.* **41**, (2024).
- [9] Y. Zhu et al., Superconductivity in pressurized trilayer  $\text{La}_4\text{Ni}_3\text{O}_{10-\delta}$  single crystals, *Nature* **631**, 531 (2024).
- [10] M. Zhang et al., Superconductivity in trilayer nickelate  $\text{La}_4\text{Ni}_3\text{O}_{10}$  under pressure, *Phys. Rev. X* **15**, 021005 (2025).
- [11] Y. Shen, M. Qin, and G.-M. Zhang, Effective bilayer model hamiltonian and density-matrix renormalization group study for the high- $T_c$  superconductivity in  $\text{La}_3\text{Ni}_2\text{O}_7$  under high pressure, *Chin. Phys. Lett.* **40**, 127401 (2023).
- [12] Q.-G. Yang, D. Wang, and Q.-H. Wang, Possible  $s_\pm$ -wave superconductivity in  $\text{La}_3\text{Ni}_2\text{O}_7$ , *Phys. Rev. B* **108**, L140505(2023).
- [13] F. Lechermann, J. Gondolf, S. Bötzel, and I. M. Eremin, Electronic correlations and superconducting instability in  $\text{La}_3\text{Ni}_2\text{O}_7$  under high pressure, *Phys. Rev. B* **108**, L201121 (2023).
- [14] V. Christiansson, F. Petocchi, and P. Werner, Correlated electronic structure of  $\text{La}_3\text{Ni}_2\text{O}_7$  under pressure, *Phys. Rev. Lett.* **131**, 206501 (2023).
- [15] Y. Gu, C. Le, Z. Yang, X. Wu, and J. Hu, Effective model and pairing tendency in the bilayer Ni-based superconductor  $\text{La}_3\text{Ni}_2\text{O}_7$ , *Phys. Rev. B* **111**, 174506 (2025).
- [16] Y.-F. Yang, G.-M. Zhang, and F.-C. Zhang, Interlayer valencebonds and two-component theory for high- $T_c$  superconductivity of  $\text{La}_3\text{Ni}_2\text{O}_7$  under pressure, *Phys. Rev. B* **108**, L201108(2023).
- [17] Q. Qin and Y.-F. Yang, High- $T_c$  superconductivity by mobilizing local spin singlets and possible route to higher  $T_c$  in pressurized  $\text{La}_3\text{Ni}_2\text{O}_7$ , *Phys. Rev. B* **108**, L140504 (2023).
- [18] Q. Qin, J. Wang, and Y.-F. Yang, Frustrated superconductivity and intrinsic reduction of  $T_c$  in trilayer nickelate, *Innov. Mater.* **2**, 100102 (2024).
- [19] X.-Z. Qu, D.-W. Qu, J. Chen, C. Wu, F. Yang, W. Li, and G. Su, Bilayer  $t$ - $J$ - $J_\perp$  model and magnetically mediated pairing in the pressurized nickelate  $\text{La}_3\text{Ni}_2\text{O}_7$ , *Phys. Rev. Lett.* **132**, 036502(2024).
- [20] H. Sakakibara, N. Kitamine, M. Ochi, and K. Kuroki, Possible high  $T_c$  superconductivity in  $\text{La}_3\text{Ni}_2\text{O}_7$  under high pressure through manifestation of a nearly-half-filled bilayer Hubbard model, *Phys. Rev. Lett.* **132**, 106002 (2024).
- [21] R. Jiang, J. Hou, Z. Fan, Z.-J. Lang, and W. Ku, Pressure driven fractionalization of ionic spins results in cuprate-like high- $T_c$  superconductivity in  $\text{La}_3\text{Ni}_2\text{O}_7$ , *Phys. Rev. Lett.* **132**, 126503(2024).
- [22] H. Sakakibara, M. Ochi, H. Nagata, Y. Ueki, H. Sakurai, R. Matsumoto, K. Terashima, K. Hirose, H. Ohta, M. Kato, Y. Takano, and K. Kuroki, Theoretical analysis on the possibility of superconductivity in the trilayer Ruddlesden-Popernickelate  $\text{La}_4\text{Ni}_3\text{O}_{10}$  under pressure and its experiment examination: Comparison with  $\text{La}_3\text{Ni}_2\text{O}_7$ , *Phys. Rev. B* **109**, 144511 (2024).
- [23] C. Lu, Z. Pan, F. Yang, and C. Wu, Interlayer coupling driven high-temperature superconductivity in  $\text{La}_3\text{Ni}_2\text{O}_7$  under pressure, *Phys. Rev. Lett.* **132**, 146002 (2024).
- [24] G. Heier, K. Park, and S. Y. Savrasov, Competing  $d_{xy}$  and  $s_\pm$  pairing symmetries in superconducting  $\text{La}_3\text{Ni}_2\text{O}_7$ : LDA+FLEX calculations, *Phys. Rev. B* **109**, 104508 (2024).
- [25] Y.-H. Tian, Y. Chen, J.-M. Wang, R.-Q. He, and Z.-Y. Lu, Correlation effects and concomitant two-orbital  $s_\pm$ -wave superconductivity in  $\text{La}_3\text{Ni}_2\text{O}_7$  under high pressure, *Phys. Rev. B* **109**, 165154 (2024).
- [26] Z. Fan, J.-F. Zhang, B. Zhan, D. Lv, X.-Y. Jiang, B. Normand, and T. Xiang, Superconductivity in nickelate

- and cuprate superconductors with strong bilayer coupling, *Phys. Rev. B* **110**, 024514 (2024).
- [27] J. Chen, F. Yang, and W. Li, Orbital-selective superconductivity in the pressurized bilayer nickelate  $\text{La}_3\text{Ni}_2\text{O}_7$ : An infinite projected entangled-pair state study, *Phys. Rev. B* **110**, L041111(2024).
- [28] K. Jiang, Z. Wang, and F. Zhang, High temperature superconductivity in  $\text{La}_3\text{Ni}_2\text{O}_7$ , *Chin. Phys. Lett.* **41**, 017402 (2024).
- [29] J.-R. Xue and F. Wang, Magnetism and superconductivity in the  $t$ - $J$  model of  $\text{La}_3\text{Ni}_2\text{O}_7$  under multiband Gutzwiller approximation, *Chin. Phys. Lett.* **41**, 057403 (2024).
- [30] J. Wang and Y.-F. Yang, Highly asymmetric superconducting dome and strange metallicity in  $\text{La}_3\text{Ni}_2\text{O}_7$ , *Phys. Rev. B* **111**, 014512 (2025).
- [31] Y.-F. Yang, Possible Fano effect and suppression of andreev reflection in  $\text{La}_3\text{Ni}_2\text{O}_7$ , *Chin. Phys. Lett.* **42**, 017301 (2025).
- [32] J. Wang and Y.-F. Yang, Fermi liquid and isotropic superconductivity of Hund scenario for bilayer nickelates, arXiv:2507.19301.
- [33] Z. Liu et al., Electronic correlations and partial gap in the bilayer nickelate  $\text{La}_3\text{Ni}_2\text{O}_7$ , *Nat. Commun.* **15**, 7570 (2024).
- [34] J. Yang et al., Orbital-dependent electron correlation in double-layer nickelate  $\text{La}_3\text{Ni}_2\text{O}_7$ , *Nat. Commun.* **15**, 4373 (2024).
- [35] Z. Dong et al., Visualization of oxygen vacancies and self-doped ligand holes in  $\text{La}_3\text{Ni}_2\text{O}_{7-\delta}$ , *Nature* **630**, 847 (2024).
- [36] X. Chen et al., Electronic and magnetic excitations in  $\text{La}_3\text{Ni}_2\text{O}_7$ , *Nat. Commun.* **15**, 9597 (2024).
- [37] H. Li, X. Zhou, T. Nummy, J. Zhang, V. Pardo, W. E. Pickett, J. F. Mitchell, and D. S. Dessau, Fermiology and electron dynamics of trilayer nickelate  $\text{La}_4\text{Ni}_3\text{O}_{10}$ , *Nat. Commun.* **8**, 704 (2017).
- [38] Z. Luo, X. Hu, M. Wang, W. Wú, and D.-X. Yao, Bilayer two-orbital model of  $\text{La}_3\text{Ni}_2\text{O}_7$  under pressure, *Phys. Rev. Lett.* **131**, 126001 (2023).
- [39] Y. Cao and Y.-F. Yang, Flat bands promoted by Hund's rule coupling in the candidate double-layer high-temperature superconductor  $\text{La}_3\text{Ni}_2\text{O}_7$  under high pressure, *Phys. Rev. B* **109**, L081105 (2024).
- [40] P.-F. Tian, H.-T. Ma, X. Ming, X.-J. Zheng, and H. Li, Effective model and electron correlations in trilayer nickelate superconductor  $\text{La}_4\text{Ni}_3\text{O}_{10}$ , *J. Phys.: Condens. Matter* **36**, 355602(2024).
- [41] C.-Q. Chen, Z. Luo, M. Wang, W. Wú, and D.-X. Yao, Trilayer multi-orbital models of  $\text{La}_4\text{Ni}_3\text{O}_{10}$ , *Phys. Rev. B* **110**, 014503(2024).
- [42] Y.-F. Yang, Decomposition of multilayer superconductivity with interlayer pairing, *Phys. Rev. B* **110**, 104507 (2024).
- [43] M. Mayr, G. Alvarez, C. Şen, and E. Dagotto, Phase fluctuations in strongly coupled  $d$ -wave superconductors, *Phys. Rev. Lett.* **94**, 217001 (2005).
- [44] Y. Dubi, Y. Meir, and Y. Avishai, Nature of the superconductor-insulator transition in disordered superconductors, *Nature* **449**, 876 (2007).
- [45] M. Karmakar, Pauli limited  $d$ -wave superconductors: quantum breached pair phase and thermal transitions, *J. Phys. Condens. Matter* **32**, 405604 (2020).
- [46] K. Pasrija, P. B. Chakraborty, and S. Kumar, Effective Hamiltonian based Monte Carlo for the BCS to BEC crossover in the attractive Hubbard model, *Phys. Rev. B* **94**, 165150 (2016).
- [47] J.-J. Dong, D. Huang, and Y.-F. Yang, Mutual information, quantum phase transition, and phase coherence in Kondo systems, *Phys. Rev. B* **104**, L081115 (2021).
- [48] A. Mukherjee, N. D. Patel, S. Dong, S. Johnston, A. Moreo, and E. Dagotto, Testing the Monte Carlo-mean field approximation in the one-band Hubbard model, *Phys. Rev. B* **90**, 205113 (2014).
- [49] Q. Qin, J.-J. Dong, Y. Sheng, D. Huang, and Y.-F. Yang, Superconducting fluctuations and charge- $4e$  plaquette state at strong coupling, *Phys. Rev. B* **108**, 054506 (2023).
- [50] Y. W. Zhong, T. Li, and Q. Han, Monte Carlo study of thermal fluctuations and Fermi-arc formation in  $d$ -wave superconductors, *Phys. Rev. B* **84**, 024522 (2011).
- [51] D. K. Singh, S. Kadge, Y. Bang, and P. Majumdar, Fermi arcs and pseudogap phase in a minimal microscopic model of  $d$ -wave superconductivity, *Phys. Rev. B* **105**, 054501 (2022).
- [52] J.-J. Dong and Y.-F. Yang, Development of long-range phase coherence on the Kondo lattice, *Phys. Rev. B* **106**, L161114 (2022).
- [53] Q. Qin and Y.-F. Yang, Intrinsic constraint on  $T_c$  for unconventional superconductivity, *npj Quantum Mater.* **10**, 13 (2025).
- [54] P. Coleman, *Introduction to Many-body Physics*, (Cambridge University Press, Cambridge, U.K., 2015).
- [55] V. J. Emery and S. A. Kivelson, Importance of phase fluctuations in superconductors with small superfluid density, *Nature* **374**, 434 (1995).
- [56] B. Keimer, S. A. Kivelson, M. R. Norman, S. Uchida, and J. Zaanen, From quantum matter to high-temperature superconductivity in copper oxides, *Nature* **518**, 179 (2015).
- [57] M. Xu et al., Anisotropic phase stiffness in infinite-layer nickelates superconductors, *Nat. Commun.* **16**, 6780 (2025).
- [58] X. B. Cheng et al., Electronic nematicity in interface superconducting LAO/KTO(111), *Phys. Rev. X* **15**, 021018 (2025).